Supporting Information

Significant enhancement of cathode-ray scintillating for a conductive Bi-*S*MOF via *in situ* partial rare earth ion replacement

Jian Lu,[ab] Xiu-Hui Zhao,[a] Bing Bai,[a] Fa-Kun Zheng*[a] and Guo-Cong Guo*[a]

[a] *State Key Laboratory of Structural Chemistry, Fujian Institute of Research on the Structure of Matter, Chinese Academy of Sciences, Fuzhou, Fujian 350002, P. R. China*

[b] *University of Chinese Academy of Sciences, Beijing, 100049, P. R. China*

Experimental section

All of the chemicals were purchased from commercial sources and were used without further purification. Organic ligand 1,4-naphthalenedicarboxylic acid (1,4-H_2ndc) and metal ion salts $Bi(NO_3)_3 \cdot 5H_2O$ and $Ln(NO_3)_3 \cdot 6H_2O$ were purchased from Adamas-beta® chemical industrial company. Organic bases imidazole and piperazine were acquired from TCI (Shanghai) chemical industry development Co., LTD. *N,N*-Dimethylformamide (DMF, 99.9%) and ethanol were from Sinopharm Chemical Reagent Co., Ltd. Ultrapure water was self-prepared and used throughout all experiments.

Synthesis of Bi-*S*MOF (1)

Compound **1** was synthesized through solvothermal reactions. $Bi(NO_3)_3 \cdot 5H_2O$ (73 mg, 0.15 mmol), 1,4-H_2ndc (216 mg, 1 mmol), and organic base (piperazine or imidazole, 0.15 mmol) were mixed and dissolved in DMF (4 mL) after vigorously stirring for 40 min. The resulting pale clear solution was transferred into a 25 mL Teflon-lined stainless vessel under autogenous pressure, then heated to 90 °C for 3 d and naturally cooled to room temperature. Block crystals of **1** were separated by filtration, washed by DMF and dried in air. Yield: 108 mg (86 % based on $Bi(NO_3)_3 \cdot 5H_2O$). The $Hdma^+$ cations are generated via the decomposition of DMF.[1-4] Elemental analysis calcd) of $C_{32}H_{34}BiN_3O_{10}$: C 46.33, H 4.13, N 5.07%, and found: C 45.87, H 4.08, N 5.22%. Selected FT-IR (cm^{-1}): 3047(m), 2965(w), 2926(w), 2789(m), 2486(w), 1656(s), 1590(s), 1557(s), 1514(s), 1461(s), 1400(s), 1368(s), 1260(s), 1202(s), 1156(m), 1103(s), 1060(w), 1025(m), 975(w), 921(m), 873(m), 836(s), 788(s), 665(s), 613(w), 574(s), 514(w) and 464 (m) (**Fig. S4**). IR bands at 1656 and 464 cm^{-1} are assigned to the carboxylate group and metal-carboxylate bond, respectively, providing information on the deprotonated ligand 1,4-ndc^{2-} and successful synthesis of **1**.

In situ doping minor RE^{3+} cations in Bi-*S*MOF 1 (RE^{3+} = Eu^{3+}, Tb^{3+}, Sm^{3+} and Dy^{3+})

The reaction process of RE^{3+} ions-doped **1a-1d** is the same as that of Bi-*S*MOF **1**, except that the initial reactant metal sources were replaced by the mixture of $Bi(NO_3)_3 \cdot 5H_2O$ (0.14625 mmol, 97.5 mol-%) and dopant $Ln(NO_3)_3 \cdot 6H_2O$ (0.00375 mmol, 2.5mol-%). After vigorously stirring for 40 minutes, the resulting pale clear solution was transferred into a 25 mL Teflon-lined stainless vessel under autogenous pressure, then heated to 90 °C for 3 days and naturally cooled to room temperature. The ICP-OES results of the mass ratio / molar ratio of Bi^{3+} and RE^{3+} are listed in **Table S4.**

X-ray crystallography

Single-crystal X-ray diffractions of **1** was performed by a Rigaku PILATUS CCD diffractometer equipped with graphite-monochromated Mo K_α radiation (λ = 0.71073 Å) at 293 K. The intensity data sets were collected using a ω-scan technique and reduced using *CrysAlisPro* software. The structures were solved by direct methods, and the subsequent successive difference Fourier syntheses yielded other nonhydrogen atoms. All atoms except hydrogen atoms were performed through the anisotropic refinement. The hydrogen atoms were calculated in the idealized positions and refined with riding coordinates on their parent atoms. The final structures were refined using a full-matrix least-squares refinement on F^2 with the Olex2 1.2 program.[5-7] The coordinated DMF molecule was refined by split process based on the actual situation. Pertinent crystal data and structure refinements are summarized in **Table S1**. The selected bond lengths and angles are listed in **Tables S2**. Hydrogen bond information is given in **Table S3**.

Physical characterization

Powder X-ray diffraction patterns (PXRD) were recorded with a Miniflex 600 at 40 kV, 40 mA for Cu-Kα with a scan speed of 0.10 s per step and a step size of 0.02 °, the data were collected within 2θ range of 5–60 °. The Mercury Version 4.1.0 software (https://www.ccdc.cam.ac.uk/support-and-resources/Downloads/#8a6058f8-d386-e511-91c5-005056868fc8_ce657cfc-4cbd-e611-807a-005056868fc8_collapse) was utilized to achieve simulated PXRD patterns dependent on the X-ray crystallographic structure. Fourier transform

infrared spectra (FT-IR) were measured with KBr slices from 4000 to 400 cm^{-1} using a VERTEX70 infrared spectrum radiometer. Solid state UV-visible diffuse reflectance spectrum was taken by PerkinElmer Lambda 365, while the absorption spectra were conducted under dilute solution state by Shimadzu UV2600 spectrophotometer. Thermogravimetric analysis (TGA) was measured using a METTLER TOLEDO system at a heating rate of 10 K min^{-1} under nitrogen atmosphere. Inductively Coupled Plasma Optical Emission Spectra (ICP-OES) were recorded on Ultima2 with the limit of detection of 0.5 ppb.

Luminescent measurements

The photoluminescence spectra were recorded on an Edinburgh FL920 phosphorimeter using a 450W Xenon lamp as excitation source. Luminescence lifetime measurements are carried out on an Edinburgh FLS920 phosphorimeter using a nanosecond pulse lamp as excitation source. The quantitative value of lifetime is calculated by exponential decay fitting.

Scintillating measurements

The cathode-ray stimulated luminescence (CL) spectra were recorded on a SEM equipped with a Gatan MonoCL3+ cathodoluminescence spectrometer and collected data was processed with the Gatan Digital Micrograph CL software. The spectra were collected using a beam of 0.9 nA and an accelerating voltage of 20 kV. The samples were aligned using the SEM to image the sample at a magnification of 100X–500X for a moderate view, and were arranged at a working distance of 12.354 nm. Spectra were obtained using 0.3 nm slit widths with collecting range from 200–800 nm.

Electrochemical measurements

The electrochemical properties of target **1**, **1a** and **1c** were evaluated in a common three-electrode cell using chronoamperometry (CA) techniques. The current densities in the present study were all obtained at –1.7V vs $Hg/HgCl_2$. All electrochemical experiments were carried out at room temperature, and all solutions were deaerated by purging with high purity Ar for 10 min

before measurements.

Calculation of electronic structures and density of states (DOS)

The calculation models were built directly from X-ray crystallographic data to calculate the energy band structures. Calculations of the electronic structures and DOS were carried out by the CASTEP code based on DFT with GGA-PBE functional in the Materials Studio v7.0 software package.[8] Energy cutoff was determined to be 750 eV, and numerical integration of Brillouin zone was employed by 2 * 2 * 1 monkhorst-Pack □-point.

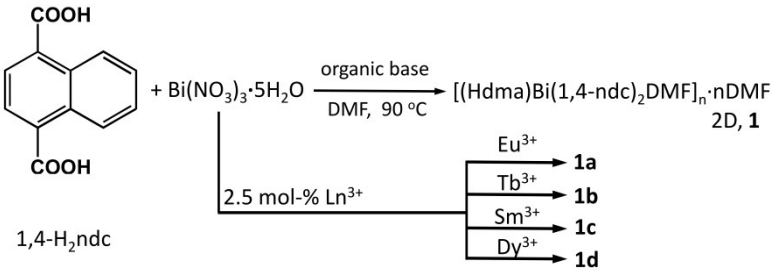

Scheme S1 The synthetic route of **1** and **1a-1d**.

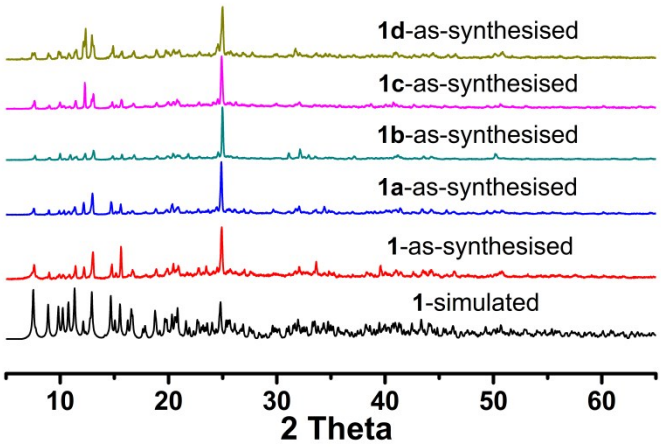

Fig. S1 The PXRD patterns of **1** and **1a-1d**.

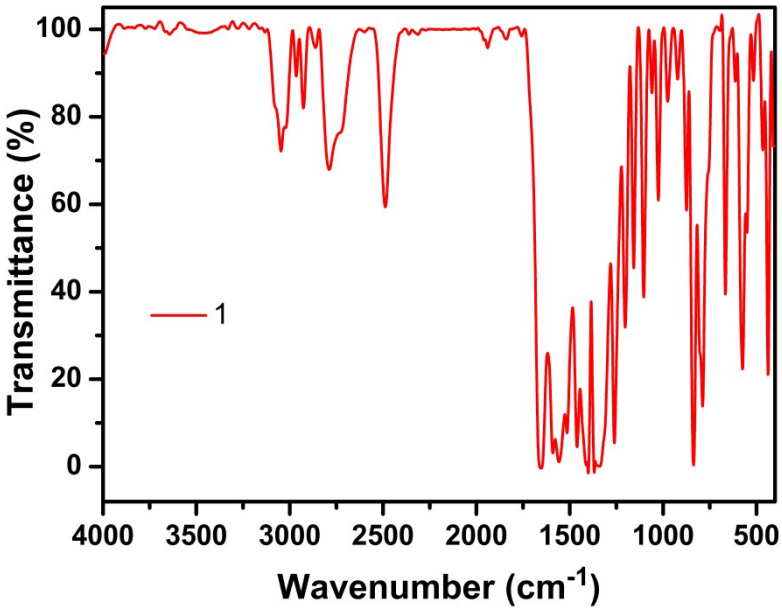

Fig. S2 The FT-IR curve of **1**.

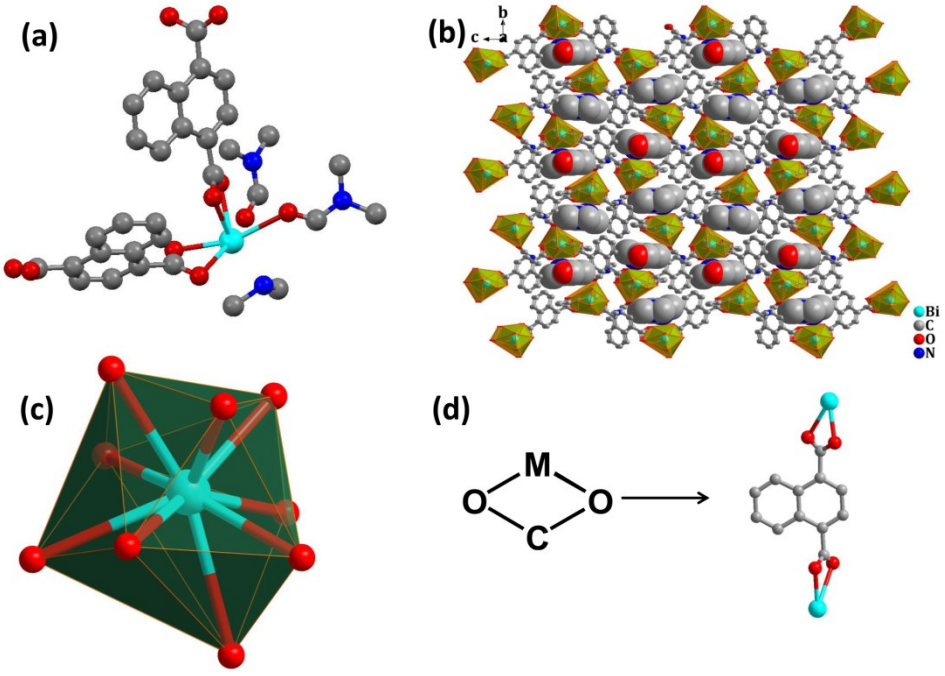

Fig. S3 For **1**: the asymmetric unit (a), the 3D supramolecular network packed by 2D Bi-ndc layers with lattice DMF and $Hdma^{+}$ filling the voids (b), the geometrical configuration around Bi(III) (c), and the chelate mode of the carboxylate group of the 1,4-ndc^{2-} ligand and the μ_2-coordination mode of the 1,4-ndc^{2-} ligand itself (d).

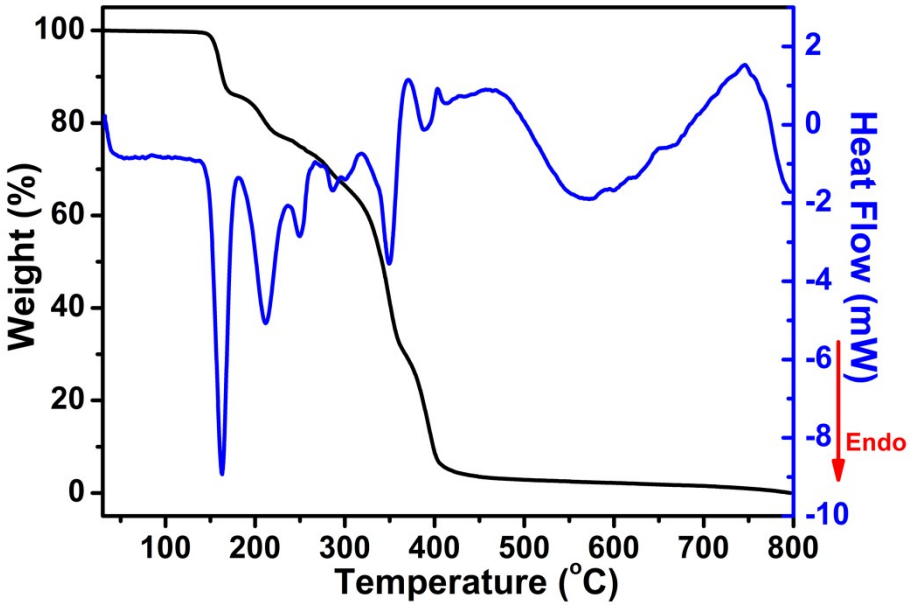

Fig. S4 The TG-DSC curves of **1**.

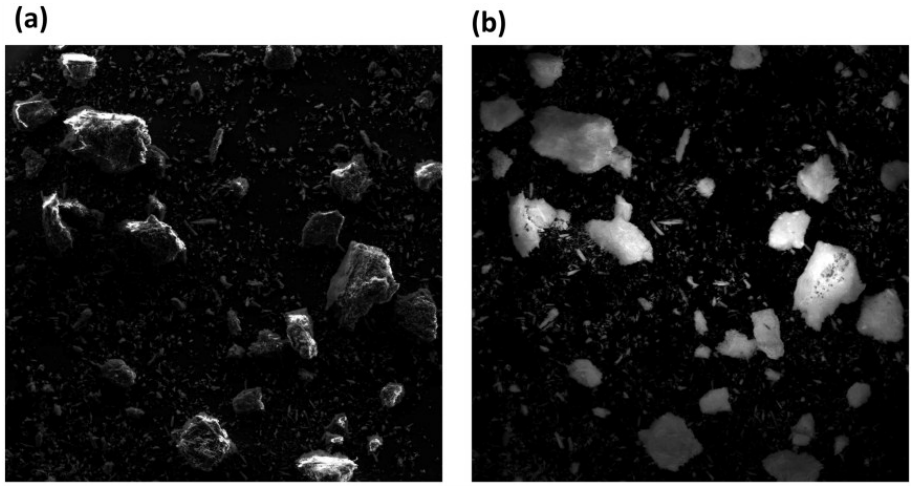

Fig. S5 The morphology of ground 1,4-H_2ndc samples (a) and its cathode-ray luminescent merits under cathode ray (b).

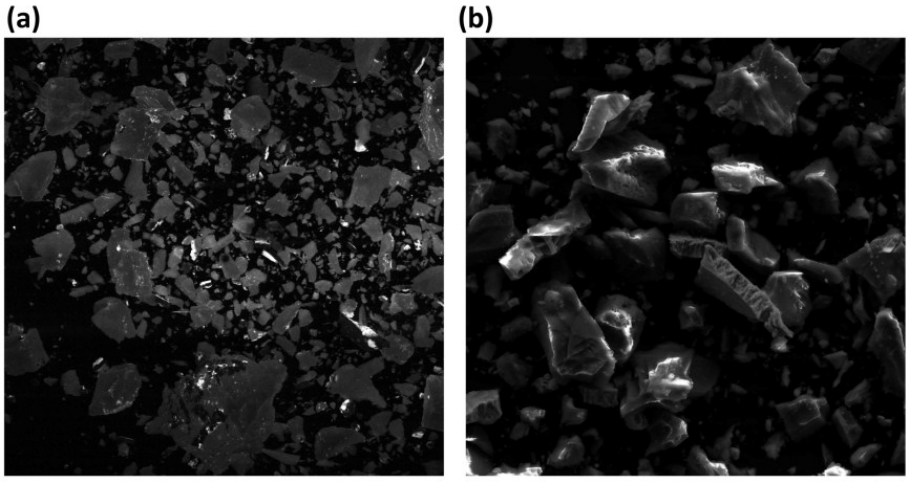

Fig. S6 The morphology of ground crystalline samples **1** (a) and its cathode-ray luminescent merits under cathode ray (b).

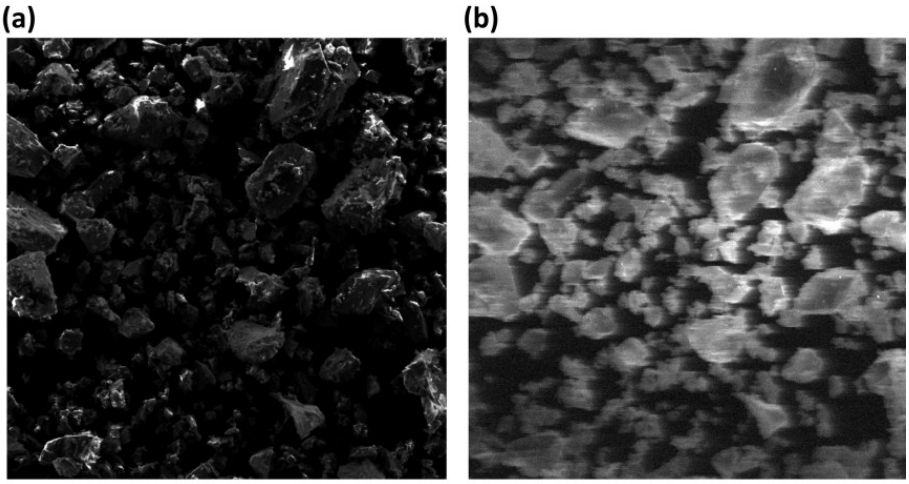

Fig. S7 The morphology of ground crystalline 0.28 mol-% Eu^{3+} doped **1a** (a) and its cathode-ray luminescent merits under cathode ray (b).

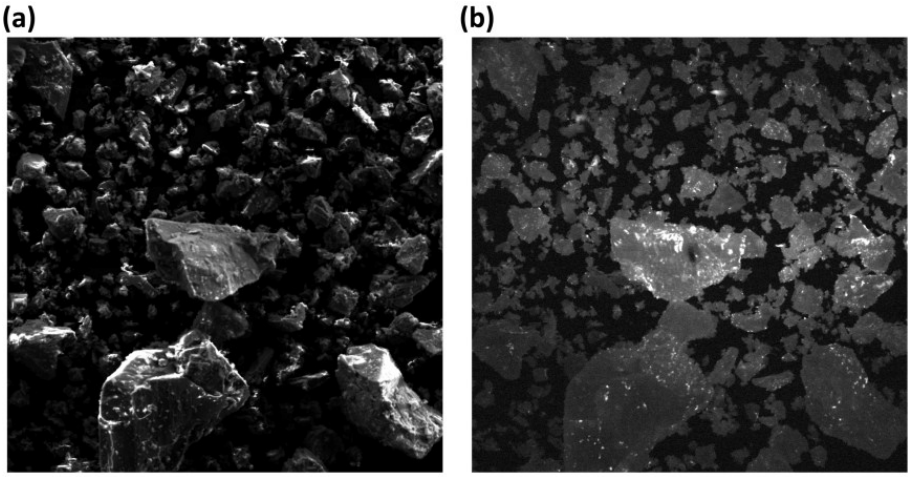

Fig. S8 The morphology of ground crystalline 1.80 mol-% Tb^{3+} doped **1b** (a) and its cathode-ray luminescent merits under cathode ray (b).

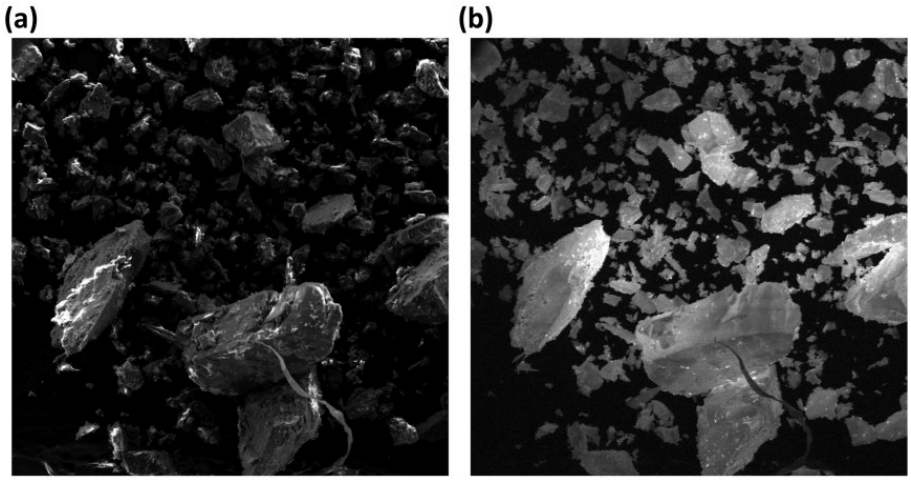

Fig. S9 The morphology of ground crystalline 0.83 mol-% Sm^{3+} doped **1c** (a) and its cathode-ray luminescent merits under cathode ray (b).

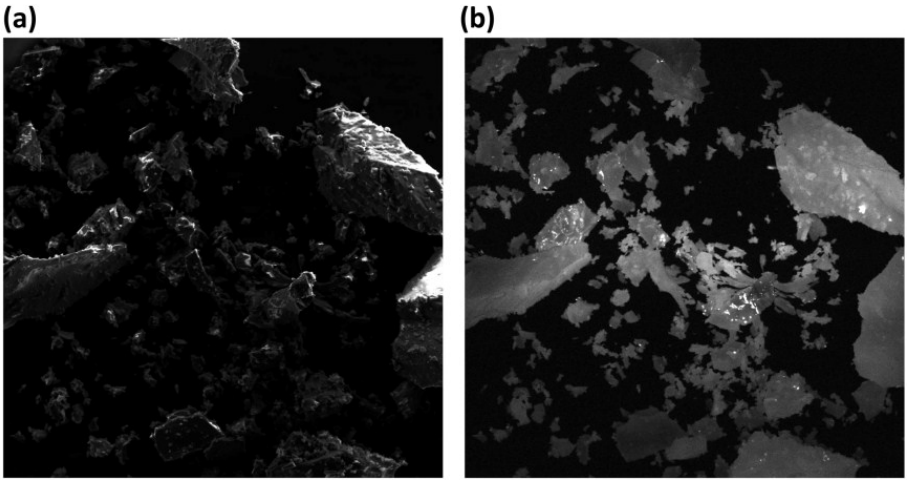

Fig. S10 The morphology of ground crystalline 2.37 mol-% Dy^{3+} doped **1d** (a) and its cathode-ray luminescent merits under cathode ray (b).

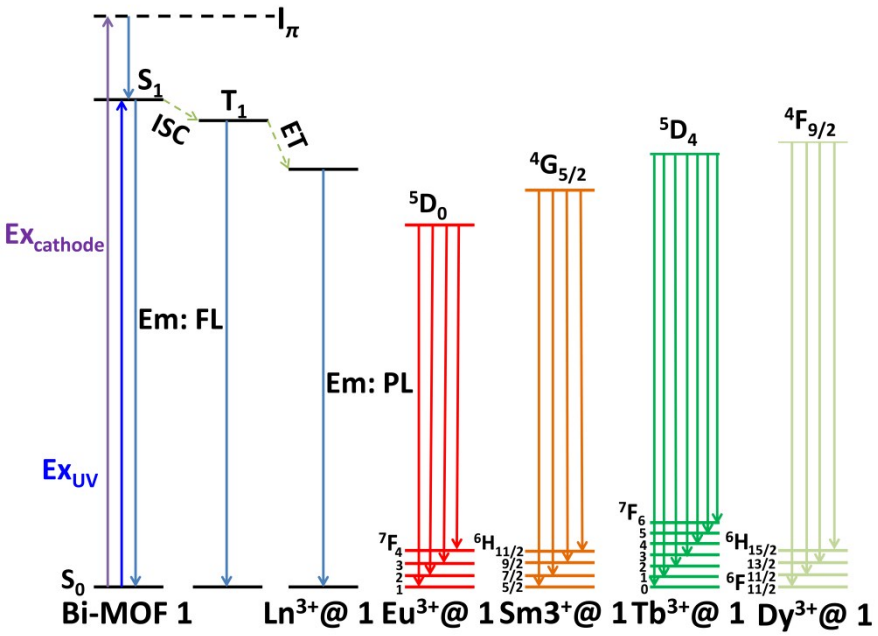

Fig. S11 Proposal mechanism for the scintillating process. FL means fluorescence while PL means phosphorescence.

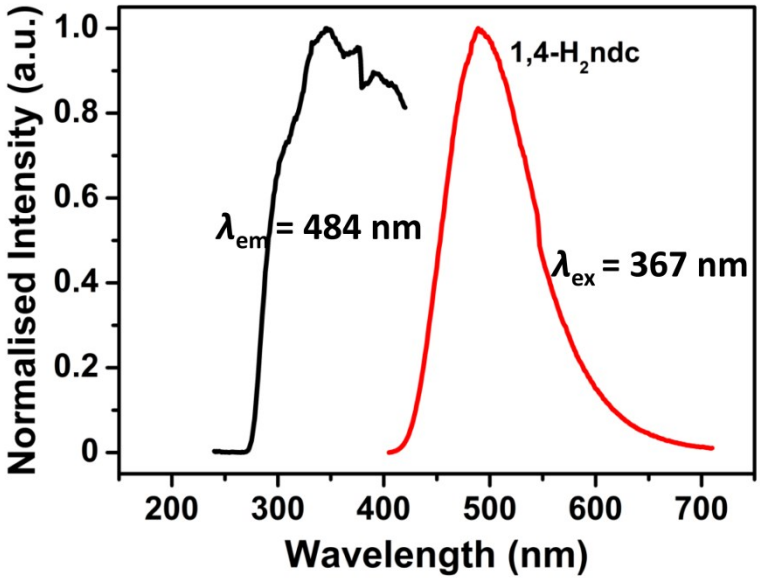

Fig. S12 The normalised solid-state steady excitation (black line) and emission (red line) spectra of free ligand 1,4-H_2ndc.

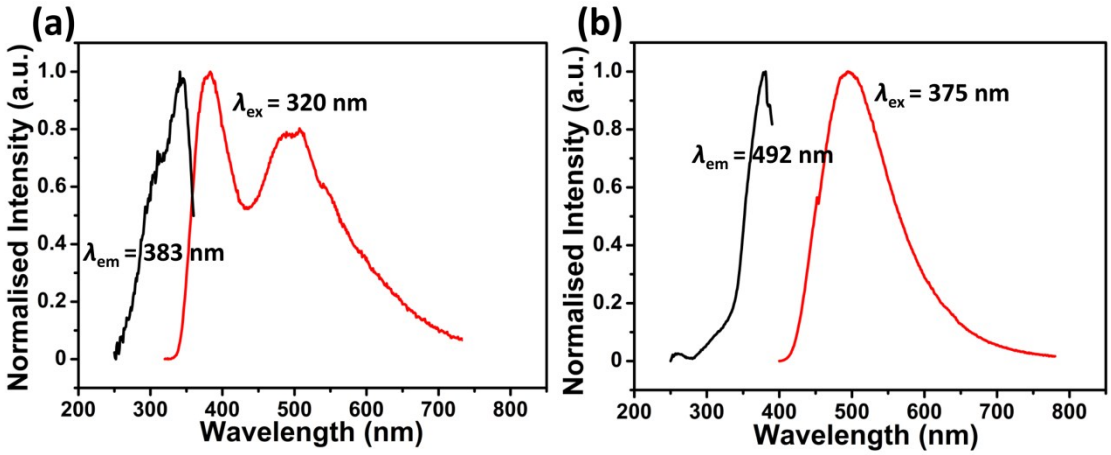

Fig. S13 The normalised solid-state steady excitation (black line) and emission (red line) spectra of **1** for LMCT (a) and intra-LCT (b) photophysical process, respectively.

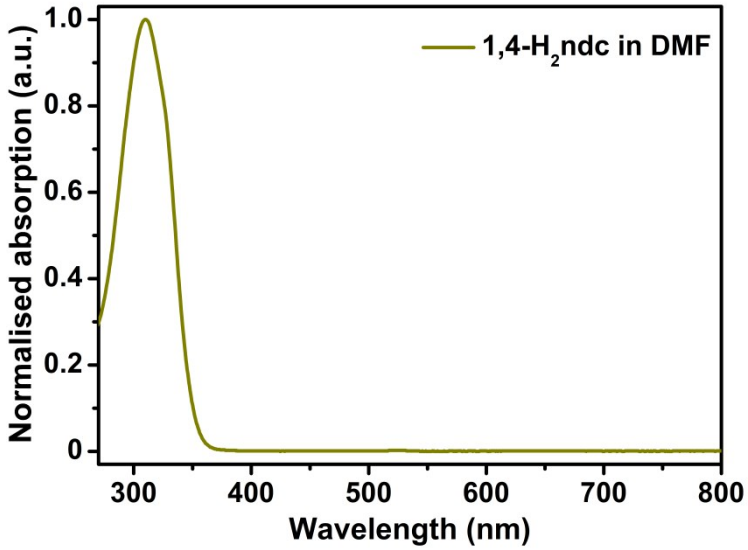

Fig. S14 The normalized UV-Vis absorption spectra of 1,4-H_2ndc in dilute DMF solvent.

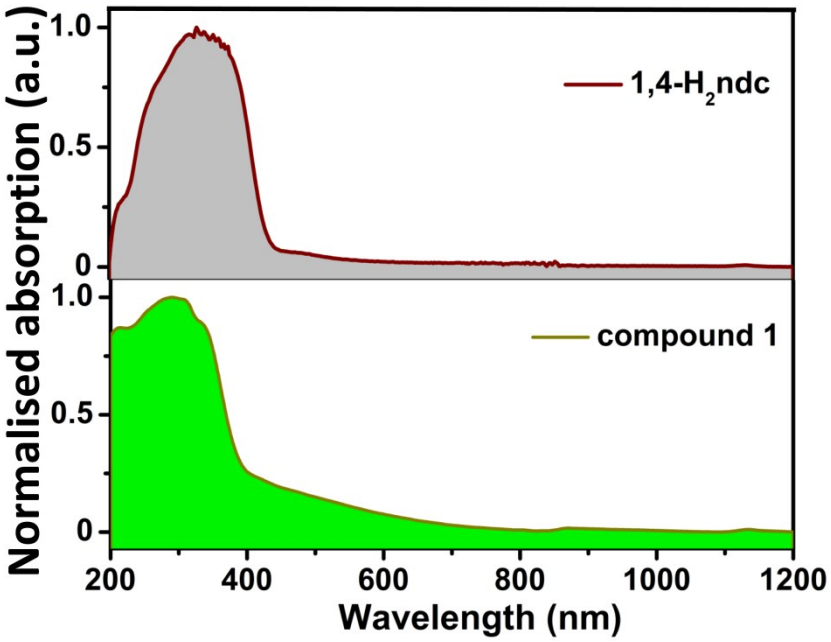

Fig. S15 The normalized solid-state UV-Vis absorption spectra of 1,4-H_2ndc and **1**, using $BaSO_4$ as the background.

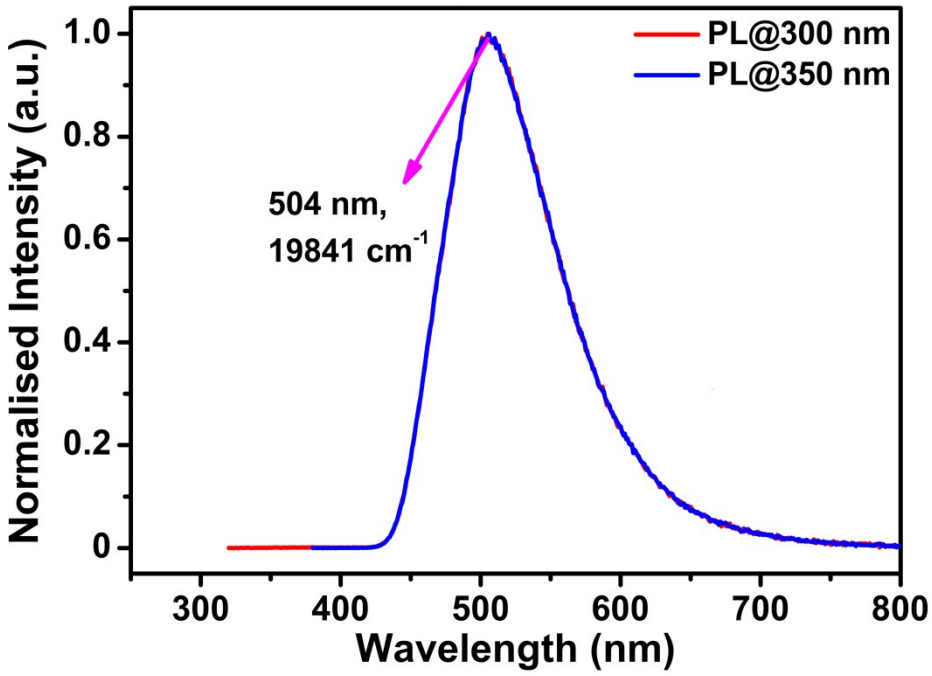

Fig. S16 The phosphorescence spectrum of 1,4-H_2ndc at 77 K, monitored by 300 and 350 nm.

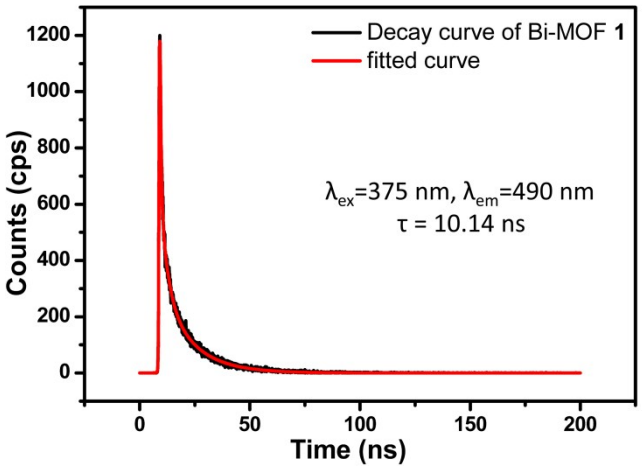

Fig. S17 The lifetime of **1** upon 375 nm excitation with their maximum emission at 490 nm under room temperature.

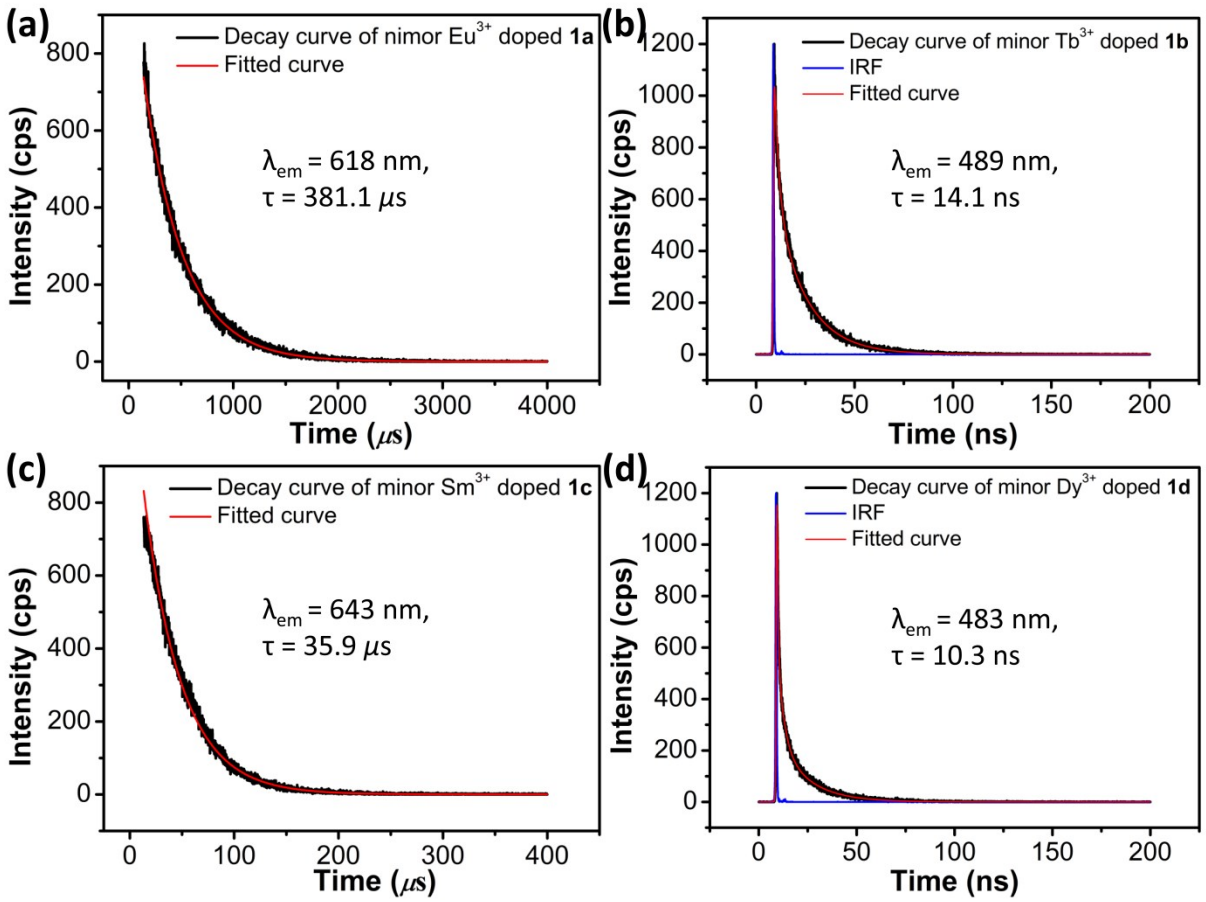

Fig. S18 The lifetimes of **1a–1d** (a-d) upon 365 nm excitation with their respective maximum emissions under room temperature.

Detailed data analysis:

$\tau_{1a} = 3.811 \times 10^{-4}$ s $\times$ 100% = 381.1 μs;

$\tau_{1b} = 2.244 \times 10^{-9}$ s $\times$ 12.41% + 1.574×10^{-8} s $\times$ 87.59% = 14.1 ns;

$\tau_{1c} = 3.593 \times 10^{-5}$ s $\times$ 100% = 35.9 μs;

$\tau_{1d} = 4.565 \times 10^{-10}$ s $\times$ 11.71% + 3.008×10^{-9} s $\times$ 23.21%+ 1.518×10^{-8} s $\times$ 65.08% = 10.3 ns;

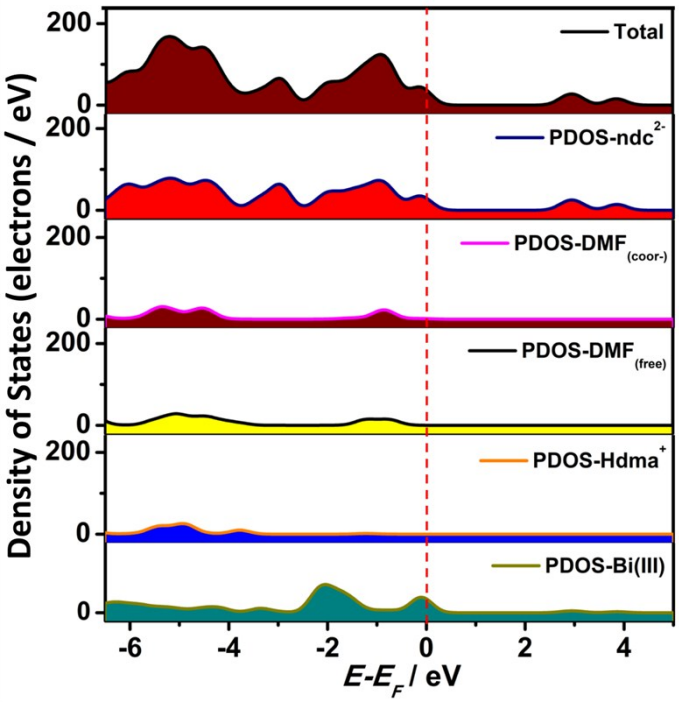

Figure S19. Total and partial density of states of **1**.

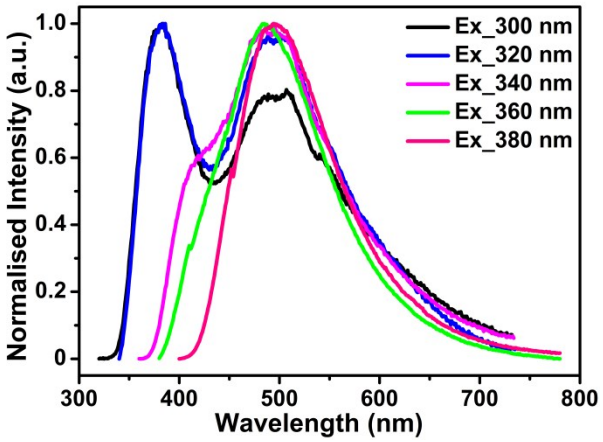

Fig. S20 The solid-state photoluminescent (PL) spectra of **1** upon excitation from 300 to 380 nm.

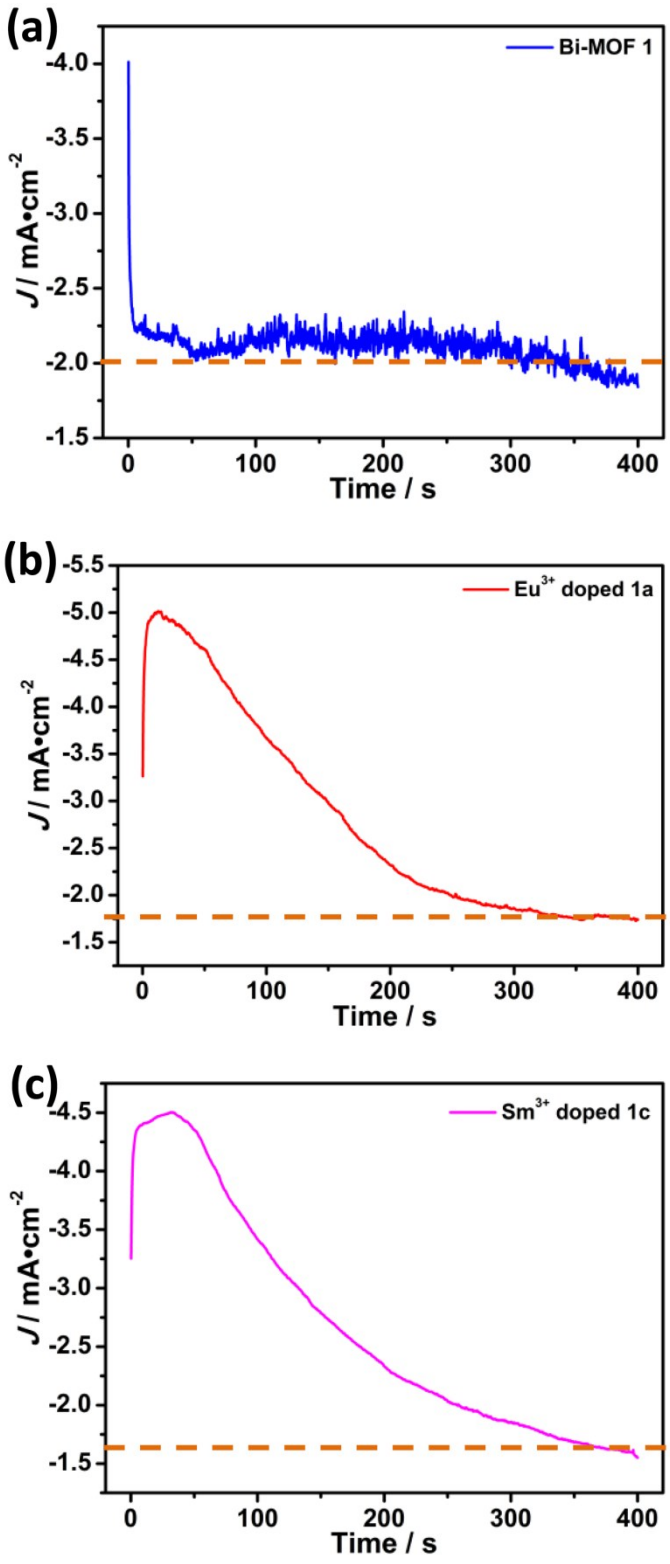

Fig. S21 The apparent current density of **1** (a), the Eu^{3+} doped **1a** (b) and Sm^{3+} doped **1c** (c).

Table S1. Crystallographic data for **1**.

Crystal data	**1**
CCDC number	1892292
Empirical formula	$C_{32}H_{34}BiN_3O_{10}$
Formula weight	829.60
Temperature	293(2)
Wavelength (Å) /MoK_α	0.71073
Crystal system	monoclinic
Space group	$P2_1/c$
a (Å)	11.5720(3)
b (Å)	14.5866(3)
c (Å)	20.1757(5)
α (°)	90
β (°)	99.824(2)
γ (°)	90
V (Å^3)	3355.64(14)
Z	4
Calcd. density (g cm^{-3})	1.640
Absorption coefficient (mm^{-1})	5.313
F(000)	1636
2θ range	7.47 to 54.99
Reflections collected	45802
Completeness to θ = 27.49°	98.9%
Data/restraints/parameters	7613/0/435
Goodness-of-fit on F^2	1.020
Final R indices [$I > 2\sigma(I)$]	R_1 = 0.0232
	wR_2 = 0.0453

[a]$R_1 = \sum(F_o - F_c)/\sum F_o$. [b]$wR_2 = [\sum w(F_o^2 - F_c^2)^2/\sum w(F_o^2)^2]^{1/2}$.

Table S2. The ICP-OES results of RE^{3+} ions-doped **1a-1d**.

Samples	Components	Mass ratio / Molar ratio
1a	Bi/Eu	19.66%:0.041% / 99.72%:0.28%
1b	Bi/Tb	19.58%:0.27% / 98.20%:1.80%
1c	Bi/Sm	19.85/0.12% / 99.17%:0.83%
1d	Bi/Dy	19.61%:0.37% / 97.63%:2.37%

Table S3. Selected bond lengths (Å) and bond angles (°) in **1**.

Bi(1)–O(1)	2.639(2)	Bi(1)–O(7)#2	2.4538(19)
Bi(1)–O(2)	2.335(2)	Bi(1)–O(8)#1	2.486(2)
Bi(1)–O(3)	2.3104(19)	Bi(1)–O(9)#1	2.3195(18)
Bi(1)–O(5)	2.703(3)		
O(1)–Bi(1)–O(5)	71.54(9)	O(7)#2–Bi(1)–O(1)	149.10(8)
O(2)–Bi(1)–O(7)#2	147.50(7)	O(7)#2–Bi(1)–O(8)#1	80.89(8)
O(2)–Bi(1)–O(1)	52.23(7)	O(7)#2–Bi(1)–O(5)	125.21(9)
O(2)–Bi(1)–O(8)#1	83.16(8)	O(8)#1–Bi(1)–O(1)	129.88(8)
O(2)–Bi(1)–O(5)	78.61(10)	O(8)#1–Bi(1)–O(5)	79.01(9)
O(3)–Bi(1)–O(9)#1	78.62(7)	O(9)#1–Bi(1)–O(7)#2	71.97(7)
O(3)–Bi(1)–O(7)#2	81.71(7)	O(9)#1–Bi(1)–O(1)	120.79(7)
O(3)–Bi(1)–O(1)	74.47(8)	O(9)#1–Bi(1)–O(2)	75.72(7)
O(3)–Bi(1)–O(2)	88.64(8)	O(9)#1–Bi(1)–O(8)#1	54.07(6)
O(3)–Bi(1)–O(5)	144.51(9)	O(9)#1–Bi(1)–O(5)	128.29(9)
O(3)–Bi(1)–O(8)#1	132.59(7)		

Symmetric codes：#1 x, 1/2 – y, 1/2 + z; #2 –1 + x, y, z; #3 x, 1/2 – y, –1/2 + z; #4 1 + x, y, z.

Table S4. Hydrogen bonds information within **1**.

D–H	A	d(D–H) (Å)	d(H…A) (Å)	∠DHA (°)	d(D…A) (Å)
N3–H3A	O10[ARU]	0.89	1.88	176	2.771(4)
N3–H3B	O7[ARU]	0.89	1.92	167	2.795(4)
C4–H4	O1	0.93	2.36	121	2.944(4)
C16–H16	O4	0.93	2.47	121	3.053(4)
C19–H19	O9	0.93	2.29	124	2.907(3)
C29–H29C	O10	0.96	2.40	104	2.794(5)

Translation of ARU-Code to CIF and Equivalent Position Code: $-x$, $1/2 + y$, $3/2 - z$.

Table S5. The main emission peaks in solid-stated cathode-ray luminescent (CL) and photoluminescent (PL) spectra of ligand 1,4-H_2ndc and **1**-**1d** at ambient temperature.

	CL (nm)	PL (nm)
1,4-H_2ndc	486	484
1	383,490	383, 490
1a	580, 594, 618, 650, 688, 696	490, 578, 593, 613, 621, 650, 688, 696
1b	376, 486	375, 489, 617
1c	388, 564, 598,644, 704	372, 562, 596, 643, 706
1d	370, 482	375, 430, 483

References

1. X.-G. Yang and D.-P. Yan, *J. Mater. Chem. C,* **2017**, *5*, 7898–7903.
2. S.-H. Yang, G.-S.B. Martin, J.-J. Titman, A.-J. Blake, D.-R. Allan, N.-R. Champness and M. Schröder, *Inorg. Chem.,* **2011**, *50*, 9374–9384.
3. G.-S. Yang, Y.-Q. Lan, H.-Y. Zang, K.-Z. Shao, X.-L. Wang, Z.-M. Su, C.-J. Jiang, *CrystEngComm.,* **2009**, *11*, 274–277.

4. C.-Y. Sun, X.-L. Wang, C. Qin, J.-L. Jin, Z.-M. Su, P. Huang, K.-Z. Shao, *Chem. Eur. J.,* **2013**, *19*, 3639 – 3645.
5. O.-V. Dolomanov, L.-J. Bourhis, R.-J. Gildea, J.-A.K. Howard and H. Puschmann, *J.Appl.Cryst*. **2009**, *42*, 339–341.
6. G.M, Sheldrick, *Acta Cryst. A*, **2015**, *71*, 3–8.
7. A. L. Spek*, J. Appl. Cryst.* **2003**. *36*, 7–13.
8. M. C. Payne, M. P. Teter, D. C. Allan, T. A. Arias, J. D. Joannopoulos, *Rev. Mod. Phys*. **1992**, *64*, 1045–1097.